ELSEVIER

Journal of Fluids and Structures 26 (2010) 176–192

JOURNAL OF FLUIDS AND STRUCTURES

www.elsevier.com/locate/jfs

# Elastic responses of a flotation ring in water waves

Guo-hai Dong[a,*], Shuang-hu Hao[b], Yun-peng Zhao[a,*], Zhi Zong[c], Fu-kun Gui[d]

[a]*State Key Laboratory of Coastal and Offshore Engineering, Dalian University of Technology, Dalian, 116024 Liaoning, China*
[b]*China Offshore Oil Engineering Co. LTD., No.1078, DanJiang Road, Tanggu, Tianjin, P.O. BOX 616, 300451, China*
[c]*School of Naval Architecture, Dalian University of Technology, Dalian, 116024 Liaoning, China*
[d]*Marine Science and Technology School, Zhejiang Ocean Univercity, Zhoushan 316000, China*

Received 4 September 2008; accepted 15 September 2009
Available online 28 October 2009

**Abstract**

The gravity-type fish cage is extensively applied in open-sea fishery aquaculture. Its practicality is closely related to the reliability of the flotation ring which is its main load-bearing component. Therefore, it is necessary to study the elastic responses of the flotation ring in ocean waves. Here, an analytical method is proposed to analyze the elastic deformations of a circular ring subjected to water waves. The governing equations of six degree-of-freedom motions and elastic deformations are obtained according to Euler's laws and curved beam theory. In order to examine the method, a series of physical model tests were carried out. The surge and heave displacements of the ring between the predicted results and experimental measurements are compared, and good correlation is represented. The effects of the propagation directions of the incident wave on elastic responses of the ring are then analyzed. It is concluded that small deformations of the ring occur when the configuration of the mooring cables is symmetrically arranged along the propagation direction of the incident waves. Additionally, the out-of-plane stiffness is suggested to be strengthened in order to diminish the corresponding deformations.


*Keywords:* Floating ring; Rigid-body motion; Elastic deformation; Morison formula

## 1. Introduction

The near-shore fishery resources decrease exponentially, while the demands of the sea products continue to dramatically increase. This imbalance in the demand–supply of marine resources has resulted in the fast development of deep-sea fishery aquaculture over recent years. Vast open space and access to quality water are the main advantages of deep-sea fishery aquaculture over its near-shore counterpart, thus enabling the former to be one of the most probable modes of fishery. Among a variety of deep-sea fishery production tools, the gravity-type deep-sea fish cage distinguishes itself from others for its high quality, high yield and high efficiency.

Generally speaking, the gravity-type net cage consists of three main components: a flotation ring, a cage net and mooring cables. The flotation ring is the load-bearing component, providing the necessary strength of the entire cage in water. The cage net is connected to the flotation ring, forming a closed space in water, inside which the fish are fed. Through the mooring cables, the cage is loosely fixed in a particular spot in the deep sea.

*Corresponding authors. Tel.: +86 411 84706031; fax: +86 411 84708526.
*E-mail addresses:* Ghdong@dlut.edu.cn (G.-h. Dong), zhaoyp18@hotmail.com (Y.-p. Zhao).

0889-9746/$ - see front matter © 2009 Elsevier Ltd. All rights reserved.
doi:10.1016/j.jfluidstructs.2009.09.001

Deep sea is characteristically rough. Under the action of waves, a deep-water fish cage may experience large deformations as well as rigid-body motions. Site observations have confirmed that a deep-water fish cage may deform to such a large extent that permanent deformations occur, disabling the fish cage from further normal functionality [Internet Webpage]. Therefore, studies of fish cages in waves have been a hot research topic over the recent years in the field of ocean hydrodynamics. Fredriksson (2001) carried out dynamic analysis of a central spar fish cage in waves. DeCew et al. (2005) examined motion and load responses of a modified gravity-type cage in order to improve the design of the gravity-type fish cage and mooring system. Both numerical simulations and physical tests were employed in their studies. Gui (2006) studied the hydrodynamic behavior of a gravity-type fish cage through physical model tests. Huang et al. (2006) proposed a numerical model for analyzing the motions of a gravity-type fish cage composed of a flexible net and a plastic flotation ring. Fredriksson et al. (2007) predicted the critical loading of net pen flotation structures using finite-element modeling, and conducted the physical tests for the structural analysis. Furthermore, Det Norske Veritas Riflex software has been used to model a fish farm.

Much of the aforementioned work is, however, based on the assumption that the load-bearing component floatation ring of the fish cage is rigid, undergoing no deformations. Thus, in their models, only the rigid-body motions of the flotation ring in waves are considered. This assumption is a first-order approximation, which may fail when the natural frequencies of the floatation ring and the water waves are similar. From the viewpoint of structural dynamics, the elastic response of the flotation ring in water waves is of vital importance. The aim of this paper is to study the elastic response of the flotation ring. And the elastic response of the slender structure is a hot topic in ocean engineering. Li et al. (1997) analyzed the in-line response of a horizontal flexibly mounted cylinder in regular and random waves. Galper and Miloh (2000) studied the nonlinear coupled hydroelastic problem of a flexible slender structure embedded in a non-uniform flow. Chaplin and Retzler (2001) carried out large-scale laboratory measurements of the hydrodynamic damping of vertical oscillations of a circular cylinder beneath waves.

In this paper, the flotation ring is simplified into a circular ring. A theoretical model is proposed to study its elastic deformation, in which, the cage net is neglected without loss of generality. Herein the in-plane and out-of-plane deformations are analyzed together based on curved beam theory. Additionally, six-degree-of-freedom motions of the ring are coupled with its elasticity. In Section 2, the equations governing the rigid-body motions are given according to Euler's laws, and those governing in-plane and out-of-plane deformations are obtained by curved beam theory. Generally speaking, the deformations of a closed ring can be expressed as a weighted sum of various eigenmodes, and the mode superposition method is applied to solve the governing equations. To calculate the wave forces acting on the ring, the Morison formula is used due to the small ratio of the cross-sectional diameter to wavelength. When waves propagate along the $x$-axis, the correlation of numerical results of surge and heave displacements with experimental data has been made in Section 4, and numerical examples are presented to show the influence of elastic deformations, including effects of propagation directions of the incident wave.

## 2. Formulation of the problem

The configuration of a gravity-type fish cage is shown in Fig. 1, where the subtended angle is denoted by $\alpha$. Points A, B, C and D are attachment points, and Points A′, B′, C′ and D′ are anchored points. The cage net is neglected without loss of generality. The flotation ring is moored by four lines in order to place the ring in a loosely fixed spatial position. Fig. 2 shows the global coordinate system $x$–$y$–$z$ fixed in the initial position and body coordinate system 1–2–3 fixed with the ring. The coordinates of one system can be transformed to the other by the use of Bryant angles (Wittenburg, 1977) $\theta_1$, $\theta_2$ and $\theta_3$ (see Appendix 1). The transformation matrix from the coordinate system $x$–$y$–$z$ to the coordinate system 1–2–3 is given as follows:

$$\begin{bmatrix} q_{11} & q_{12} & q_{13} \\ q_{21} & q_{22} & q_{23} \\ q_{31} & q_{32} & q_{33} \end{bmatrix} = \begin{bmatrix} \cos\theta_2\cos\theta_3 & \cos\theta_1\sin\theta_3+\sin\theta_1\sin\theta_2\cos\theta_3 & \sin\theta_1\sin\theta_3-\cos\theta_1\sin\theta_2\cos\theta_3 \\ -\cos\theta_2\sin\theta_3 & \cos\theta_1\cos\theta_3-\sin\theta_1\sin\theta_2\sin\theta_3 & \sin\theta_1\cos\theta_3+\cos\theta_1\sin\theta_2\sin\theta_3 \\ \sin\theta_2 & -\sin\theta_1\cos\theta_2 & \cos\theta_1\cos\theta_2 \end{bmatrix}, \tag{1}$$

where $q$ with subscripts denotes the corresponding terms in the transformation matrix. It is noted that $\theta_1$, $\theta_2$ and $\theta_3$ are *not* the rotation angles of roll, pitch and yaw of the ring. Here the angular velocities of 1-, 2-and 3-axis are denoted by $\omega_1$, $\omega_2$ and $\omega_3$, respectively. The relationship is as follows:

$$\begin{aligned} &\frac{\partial\theta_1}{\partial t}=\frac{\omega_1\cos\theta_3-\omega_2\sin\theta_3}{\cos\theta_2}, \frac{\partial\theta_2}{\partial t}=\omega_1\sin\theta_3+\omega_2\cos\theta_3 \\ &\frac{\partial\theta_3}{\partial t}=\omega_3-\frac{\omega_1\cos\theta_3-\omega_2\sin\theta_3}{\cos\theta_2}\sin\theta_2 \end{aligned} \tag{2}$$

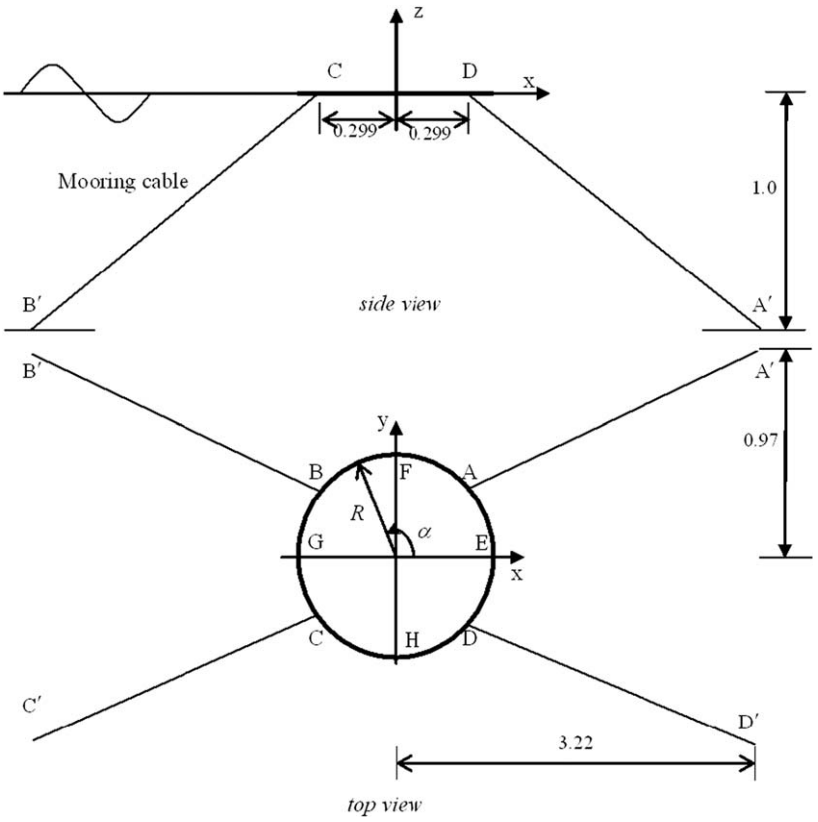


Fig. 1. The configuration of a fish cage.

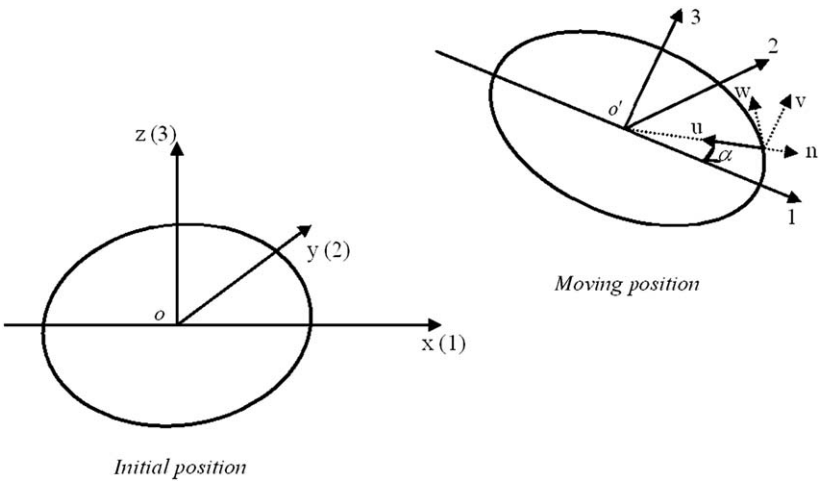


Fig. 2. The coordinate system of the ring.

In addition, the in-plane coordinate system $n$–$w$–$v$ is established, in which the coordinate area $n$–$w$ results from the rotation of the coordinate area 1–2 around the 3-axis, and the direction of the $v$-axis is the same as that of the 3-axis. It is noted that the $u$-axis considered is opposite to the direction of the $n$-axis in order to analyze the normal deformations.

The actual flotation system of a gravity-type fish cage consists of two floating rings, stanchions and handrails. In general, the floating system is usually at the water surface. The two floating rings are the main parts bearing the

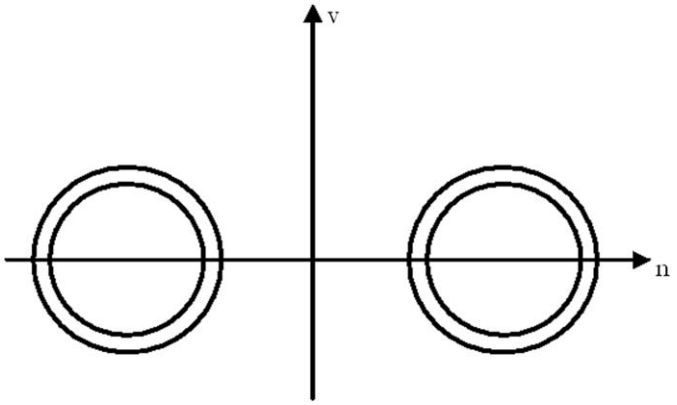


Fig. 3. Cross-section of the ring.

wave-induced loads. For simplicity, only the two floating rings are considered in our numerical model, as shown in Fig. 3. Since the space between the outer and inner rings is much smaller than the scale of the floating system and wave length, we can simplify it to a model of a single ring. The area of the cross-section and the moment of inertia, however, are computed based on two rings (see Fig. 3) to comply with the quantity of the actual flotation ring. The moments of inertia are computed according to the parallel-axis theorem.

### 2.1. Governing equations for rigid-body motions

Suppose that the wave propagates along a direction of angle $\sigma$ subtended with the $x$-axis. The ring undergoes six degree-of-freedom motions. Three translational rigid-body motion displacements along the $x$-axis for surge, the $y$-axis for sway and the $z$-axis for heave are denoted by $x_g$, $y_g$ and $z_g$, respectively. The translational displacements in the body coordinate system are denoted by $x_b$, $y_b$ and $z_b$ along the 1-axis, 2-axis and 3-axis.

The equations governing the rigid-body motions of the ring are considered along the 1-, 2- and 3-axis, because the principal moment of inertia of the ring is constant in the body coordinate system. Applying Euler's laws, the following equations can be obtained.

*Translational motions*

The translational equation along the 1-axis is

$$\rho(2\pi R)A\left(\frac{\partial^2 x_b}{\partial t^2}+\frac{\partial z_b}{\partial t}\omega_2-\frac{\partial y_b}{\partial t}\omega_3\right)=\int_0^{2\pi} f_1 R d\alpha+q_{13}\int_0^{2\pi}(\rho_w V_f g-\rho A g)Rd\alpha+F_{l1}, \tag{3}$$

where $R$ denotes the radius of the ring, $\rho$ the mass density of the material of the ring, $\rho_w$ the density of water, $A$ the cross-sectional area of the ring and $g$ the gravitational acceleration. On the right-hand side of Eq. (3), the second term is induced by the buoyancy and gravity, and $V_f$ is the wetted volume per unit length of the ring given by

$$V_f=\begin{cases}\pi r^2 & h\geq r\\ \frac{\pi r^2}{2}+|h|\sqrt{r^2-h^2}+r^2\arcsin(|h|/r) & 0\leq h\leq r\\ \frac{\pi r^2}{2}-|h|\sqrt{r^2-h^2}-r^2\arcsin(|h|/r) & -r\leq h\leq 0\\ 0 & h\leq -r\end{cases} \tag{4}$$

where $r$ is the radius of the cross-section, and $h$ the distance from the fluctuating wave surface height $\eta$ to the cross-sectional centroid of the ring,

$$h=\eta-z. \tag{5}$$

According to Euler's laws, the equations along 2-axis and 3-axis can also be obtained

$$\rho(2\pi R)A\left(\frac{\partial^2 y_b}{\partial t^2}+\frac{\partial x_b}{\partial t}\omega_3-\frac{\partial z_b}{\partial t}\omega_1\right)=\int_0^{2\pi} f_2 R d\alpha+q_{23}\int_0^{2\pi}(\rho_w V_f g-\rho A g)Rd\alpha+F_{l2}, \tag{6}$$

$$\rho(2\pi R)A\left(\frac{\partial^2 z_b}{\partial t^2}+\frac{\partial y_b}{\partial t}\omega_1-\frac{\partial x_b}{\partial t}\omega_2\right)=\int_0^{2\pi} f_3 R d\alpha+q_{33}\int_0^{2\pi}(\rho_w V_f g-\rho A g)R d\alpha+F_{l3}. \tag{7}$$

Eqs. (3), (6) and (7) are the governing equations to calculate the translational displacements, where $f_1$, $f_2$ and $f_3$ are the wave force on the ring per unit length along 1-, 2- and 3-axis, and $F_{l1}$, $F_{l2}$ and $F_{l3}$ are mooring cable forces.

*Rotational motions*

Besides the translations of the circular ring, its rotations around three axes are subjected to water waves. Through Euler's laws, the equations governing the rotations around 1-, 2- and 3-axis can be given as follows:

$$I_1\frac{\partial\omega_1}{\partial t}+(I_3-I_2)\omega_3\omega_2=\int_0^{2\pi} f_3 R\sin\alpha R d\alpha+\int_0^{2\pi} q_{33}*(\rho_w V_f g-\rho A g)R\sin\alpha R d\alpha+M_{l1}, \tag{8}$$

$$I_2\frac{\partial\omega_2}{\partial t}+(I_1-I_3)\omega_1\omega_3=-\left[\int_0^{2\pi} f_3 R\cos\alpha R d\alpha+\int_0^{2\pi} q_{33}(\rho_w V_f g-\rho A g)R\cos\alpha R d\alpha+M_{l2}\right], \tag{9}$$

$$I_3\frac{\partial\omega_3}{\partial t}+(I_2-I_1)\omega_1\omega_2=\int_0^{2\pi} f_w R*R d\alpha+\int_0^{2\pi} q_{23}(\rho_w V_f g-\rho A g)R*R\,d\alpha+F_{lw}R, \tag{10}$$

where $I_1$, $I_2$ and $I_3$ are three principal moments of inertia of the ring; $M_{l1}$ and $M_{l2}$ denote the moments induced by the mooring cable forces around 1-axis and 2-axis, respectively; $f_w$ are the wave forces per unit length of the ring along the circumferential direction, and $F_{lw}$ is a component of the mooring line force along the circumferential direction of the ring.

### 2.2. Governing equations for in-plane elastic deformations

To analyze the deformation of the ring, an element of the ring is regarded as a curved beam. As shown in Fig. 4, the in-plane elastic deformations include the circumferential deformation $w$ and radial deformation $u$. The internal forces on the cross-section include circumferential tensile force $N$, transverse shear force $Q_u$, and bending moment $M_v$ around the $v$-axis. In addition, $\phi_v$ denotes the slope of the deflection profile around the $v$-axis without considering the shear effect. Applying Newton's Second Law, three equations governing the deformations are obtained, as follows:

$$\frac{\partial Q_u}{\partial\alpha}+N+F_u=\rho AR\frac{\partial^2 u}{\partial t^2},\quad \frac{\partial N}{\partial\alpha}-Q_u-F_w=\rho AR\frac{\partial^2 w}{\partial t^2},\quad \frac{\partial M_v}{\partial\alpha}+RQ_u=\rho I_v R\frac{\partial^2\phi_v}{\partial t^2}, \tag{11}$$

where $I_v$ is the moment of inertia of the cross-section of the ring around the $v$-axis, $E$ the modulus of elasticity and $G$ the shear modulus of elasticity; $F_u$ and $F_w$ are the normal and circumferential forces

$$\begin{aligned} F_u&=[f_u R+(\rho_w\forall_f g-\rho A g)(\cos\alpha q_{13}+\sin\alpha q_{23})]Rd\alpha+F_{lu},\\ F_w&=[f_w R+(\rho_w\forall_f g-\rho A g)(-\sin\alpha q_{13}+\cos\alpha q_{23})]Rd\alpha+F_{lw}. \end{aligned} \tag{12}$$

In the integrand on the right-hand side of Eq. (12), $f_u$ and $f_w$ are wave forces in the normal and circumferential directions, respectively, and the second terms are induced by buoyancy and gravity. $F_{lu}$ and $F_{lw}$ are the normal and tangential components of mooring cable forces, respectively.

According to engineering mechanics, the bending moment and shear force are dependent on the deformations through the following formulae

$$M=\frac{EI_v}{R}\frac{\partial\phi_v}{\partial\alpha},\quad Q_u=\frac{k' AG}{R}\left(\frac{\partial u}{\partial\alpha}+w-R\phi_v\right), \tag{13}$$

where $k'$ is a correction coefficient, depending on the shape of the cross section.

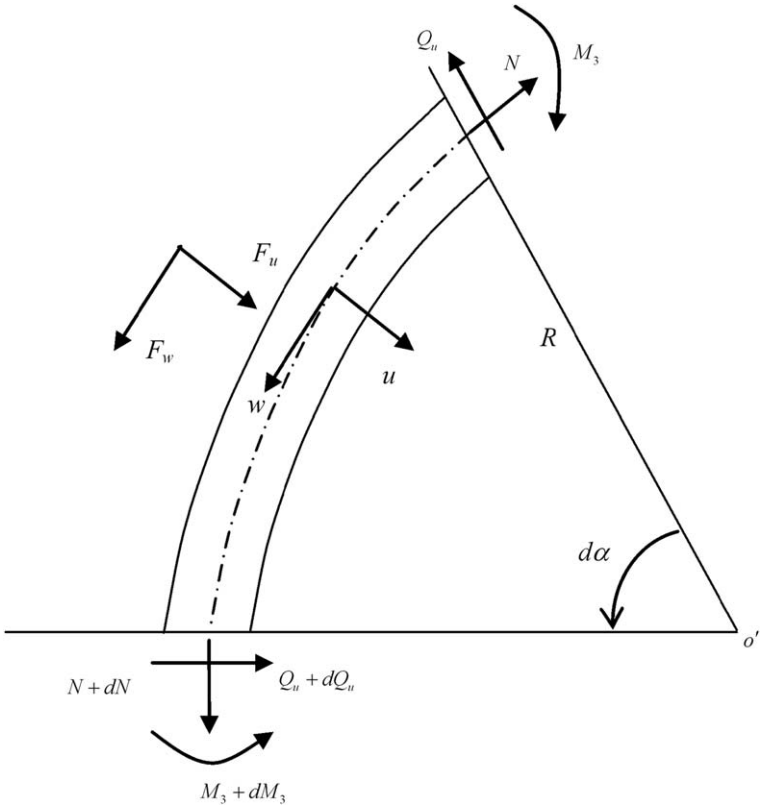


Fig. 4. In-plane deformation and internal forces for an element of the ring.

Substituting Eq. (13) into (11), the equation governing racial deformation $u$ and circumferential deformation $w$ can be obtained as follows:

$$\begin{aligned}
&\frac{\partial^5 u}{\partial\alpha^5}+\frac{\partial^4 w}{\partial\alpha^4}+\frac{\partial^3 u}{\partial\alpha^3}+\frac{\partial^2 w}{\partial\alpha^2}+\frac{\rho^2R^4}{Ek'G}\frac{\partial^5 u}{\partial t^4\partial\alpha}\\
&\quad-\left(\frac{\rho R^2}{E}+\frac{\rho R^2}{k'G}\right)\frac{\partial^5 u}{\partial t^2\partial\alpha^3}+\left(\frac{\rho AR^4}{EI_v}-\frac{\rho R^2}{E}\right)\frac{\partial^3 u}{\partial t^2\partial\alpha}\\
&\quad+\left(\frac{\rho R^2}{k'G}-\frac{\rho R^2}{E}\right)\frac{\partial^4 w}{\partial t^2\partial\alpha^2}-\left(\frac{\rho R^2}{E}+\frac{\rho AR^4}{EI_v}\right)\frac{\partial^2 w}{\partial t^2}-\frac{\rho^2R^4}{Ek'G}\frac{\partial^4 w}{\partial t^4}\\
&\quad=\frac{\rho R^3}{Ek'AG}\left(\frac{\partial^3 F_u}{\partial t^2\partial\alpha}+\frac{\partial^2 F_w}{\partial t^2}\right)+\frac{R^3}{EI_v}\left(\frac{\partial F_u}{\partial\alpha}+F_w\right)-\frac{R}{k'AG}\left(\frac{\partial^3 F_u}{\partial\alpha^3}+\frac{\partial^2 F_w}{\partial\alpha^2}\right).
\end{aligned}\tag{14}$$

Based on the assumption of small deformations, we consider that the centerline is inextensible, i.e.

$$\frac{\partial w}{\partial\alpha}=u.\tag{15}$$

By virtue of Eq. (15), Eq. (14) is reduced to containing a single variable $w$ in the form of

$$\begin{aligned}
&\frac{\partial^6 w}{\partial\alpha^6}+2\frac{\partial^4 w}{\partial\alpha^4}+\frac{\partial^2 w}{\partial\alpha^2}+\frac{\rho^2R^4}{Ek'G}\frac{\partial^6 w}{\partial t^4\partial\alpha^2}-\frac{\rho^2R^4}{Ek'G}\frac{\partial^4 w}{\partial t^4}\\
&\quad-\left(\frac{\rho R^2}{E}+\frac{\rho R^2}{k'G}\right)\frac{\partial^6 w}{\partial t^2\partial\alpha^4}-\left(2\frac{\rho R^2}{E}-\frac{\rho AR^4}{EI_v}-\frac{\rho R^2}{k'G}\right)\frac{\partial^4 w}{\partial t^2\partial\alpha^2}-\left(\frac{\rho R^2}{E}+\frac{\rho AR^4}{EI_v}\right)\frac{\partial^2 w}{\partial t^2}\\
&\quad=\frac{\rho R^3}{Ek'AG}\left(\frac{\partial^3 F_u}{\partial t^2\partial\alpha}+\frac{\partial^2 F_w}{\partial t^2}\right)+\frac{R^3}{EI_v}\left(\frac{\partial F_u}{\partial\alpha}+F_w\right)-\frac{R}{k'AG}\left(\frac{\partial^3 F_u}{\partial\alpha^3}+\frac{\partial^2 F_w}{\partial\alpha^2}\right).
\end{aligned}\tag{16}$$

The dimensionless procedure of Eq. (16) can be performed through dividing each term of both sides of the equation by $R$. The order of magnitude of $E$ and $G$ is $10^8$, of $\rho$ is $10^0$, of $A$ is $10^{-3}$, of $R$ is $10^0$, of $\omega$ is $10^0$ and of the moment of inertia is $10^{-5}$. Therefore, the order of magnitude of terms the denominators of which contain the product of $E$ and $G$ is less than $10^{-10}$, while the order of magnitude of the others is more than $10^{-5}$. Therefore, Eq. (16) can be simplified into the following form:

$$\begin{aligned}&\frac{\partial^6 w}{\partial\alpha^6}+2\frac{\partial^4 w}{\partial\alpha^4}+\frac{\partial^2 w}{\partial\alpha^2}\\&\quad-\left(\frac{\rho R^2}{E}+\frac{\rho R^2}{k'G}\right)\frac{\partial^6 w}{\partial t^2\partial\alpha^4}\\&\quad-\left(2\frac{\rho R^2}{E}-\frac{\rho AR^4}{EI_v}-\frac{\rho R^2}{k'G}\right)\frac{\partial^4 w}{\partial t^2\partial\alpha^2}-\left(\frac{\rho R^2}{E}+\frac{\rho AR^4}{EI_v}\right)\frac{\partial^2 w}{\partial t^2}\\&\quad=\frac{R^3}{EI_v}\left(\frac{\partial F_u}{\partial\alpha}+F_w\right)-\frac{R}{k'AG}\left(\frac{\partial^3 F_u}{\partial\alpha^3}+\frac{\partial^2 F_w}{\partial\alpha^2}\right).\end{aligned}\tag{17}$$

The deformations can be expressed as a weighted sum of eigenmodes when the modal superposition method is applied. Thus the circumferential deformation $w$ and radial deformation $u$ are

$$\begin{aligned}w&=\sum_{i=2}^{N}[\tau_i^s(t)\sin(i\alpha)+\tau_i^c(t)\cos(i\alpha)],\\u&=\frac{\partial w}{\partial\alpha}=\sum_{i=2}^{N}[i\tau_i^s(t)\cos(i\alpha)-i\tau_i^c(t)\sin(i\alpha)],\end{aligned}\tag{18}$$

where the subscript $i$ denotes the $i$th mode. It should be noted that the mode number $i$ begins with 2, because the 1st mode represents the rigid-body displacement. When Eq. (18) is substituted into Eq. (17) and the orthogonality of the trigonometric functions is utilized, the governing equations for each mode can be obtained as follows:

$$\begin{aligned}&\pi\rho R^2\left[(i^2-1)^2I_v+i^2(i^2+1)\frac{I_v}{k}\frac{E}{G}+(i^2+1)AR^2\right]\frac{\partial^2\tau_i^s}{\partial t^2}\\&\quad=R\left(\frac{i^2}{k}\frac{I_v}{A}\frac{E}{G}+R^2\right)\left[i\int_0^{2\pi}F_u\cos(i\alpha)d\alpha+\int_0^{2\pi}F_t\sin(i\alpha)d\alpha\right]-\pi EI_v(i^3-i)^2\tau_i^s,\end{aligned}\tag{19}$$

and

$$\begin{aligned}&\rho R^2\left[(i^2-1)^2I_v+\frac{EI_i}{kG}i^2(i^2+1)+AR^2(i^2+1)\right]\frac{\partial^2\tau_i^c}{\partial t^2}\pi\\&\quad=-R\left(R^2+\frac{EI_v}{kAG}i^2\right)\left[i\int_0^{2\pi}F_n\sin(i\alpha)d\alpha-\int_0^{2\pi}F_t\cos(i\alpha)d\alpha\right]-\pi EI_v(i^3-i)^2\tau_i^c,\quad i=2,3,\ldots,J.\end{aligned}$$

Eqs. (19) are the governing equations to compute the circumferential deformation. Then another equation governing the slope $\phi_v$ can be obtained by combining Eqs. (11) and (13), and the modal superposition method is used to represent $\phi_v$ as follows:

$$\phi_v=\sum_{i=2}^{J}[\psi_i^s(t)\sin(i\alpha)+\psi_i^c(t)\cos(i\alpha)].\tag{20}$$

Manipulating Eq. (20) by the above procedure, the governing equation for each mode can be obtained in the form of

$$\begin{aligned}&\pi\rho R^2\left[(i^2-1)^2I_v+i^2(i^2+1)\frac{I_v}{k}\frac{E}{G}+(i^2+1)AR^2\right]\frac{\partial^2\psi_i^s}{\partial t^2}\\&\quad=-R^2(i^2-1)\left[i\int_0^{2\pi}F_u\cos(i\alpha)d\alpha+\int_0^{2\pi}F_w\sin(i\alpha)d\alpha\right]-\pi EI_v(i^3-i)^2\psi_i^s,\end{aligned}\tag{21}$$

and

$$\pi\rho R^2\left[I_v(i^2-1)^2+\frac{EI_v}{kG}i^2(i^2+1)+AR^2(i^2+1)\right]\frac{\partial^2\psi_i^c}{\partial t^2}$$
$$=R^2(i^2-1)\left[i\int_0^{2\pi}F_u\sin(i\alpha)d\alpha-\int_0^{2\pi}F_w\cos(j\alpha)d\alpha\right]-(i^3-i)^2EI_v\pi\psi_i^c,\quad i=2,3,\ldots,J.$$

Eqs. (19) and (21) are then used to analyze the in-plane deformations of the ring.

### 2.3. Governing equations for out-of-plane elastic deformations

As shown in Fig. 5, the out-of-plane elastic deformations are denoted by $v$, positive along the positive direction of the $v$-axis. The internal forces on the cross-section include the transverse shear force $Q_v$, and bending moments $M_u$ and $M_w$ along the $u$-axis and $w$-axis. In addition, $\phi_u$ and $\phi_w$ denote the slope of the deflection profile around the $u$-axis and $w$-axis with the shear effect neglected. Applying Newton's Second Law, three equations governing the deformations can be obtained in the form of

$$\frac{\partial Q_v}{\partial\alpha}+F_v=\rho AR\frac{\partial^2 v}{\partial t^2},\quad \frac{\partial M_u}{\partial\alpha}+M_w-Q_vR=\rho I_uR\frac{\partial^2\phi_u}{\partial t^2},\quad \frac{\partial M_w}{\partial\alpha}-M_u=\rho I_wR\frac{\partial^2\phi_w}{\partial t^2},\tag{22}$$

where $I_u$ and $I_w$ are the moment of inertia of the cross-section of $u$-axis and $w$-axis obtained according to the parallel-axis theorem, and $F_v$ is the component of exterior forces along the $v$-axis, which is given by

$$F_v=[f_vR+q_{33}(\rho_w\forall_f g-\rho Ag)]Rd\alpha+F_{lv}.\tag{23}$$

In engineering mechanics, bending moment and shear force are dependent on the deformations through the following formula:

$$M_u=\frac{EI_u}{R}\left(\frac{\partial\phi_u}{\partial\alpha}+\phi_w\right),\quad M_w=\frac{GI_w}{R}\left(\frac{\partial\phi_w}{\partial\alpha}-\phi_u\right),\quad Q_v=\frac{k'AG}{R}\left(\frac{\partial v}{\partial\alpha}+\phi_u\right).\tag{24}$$

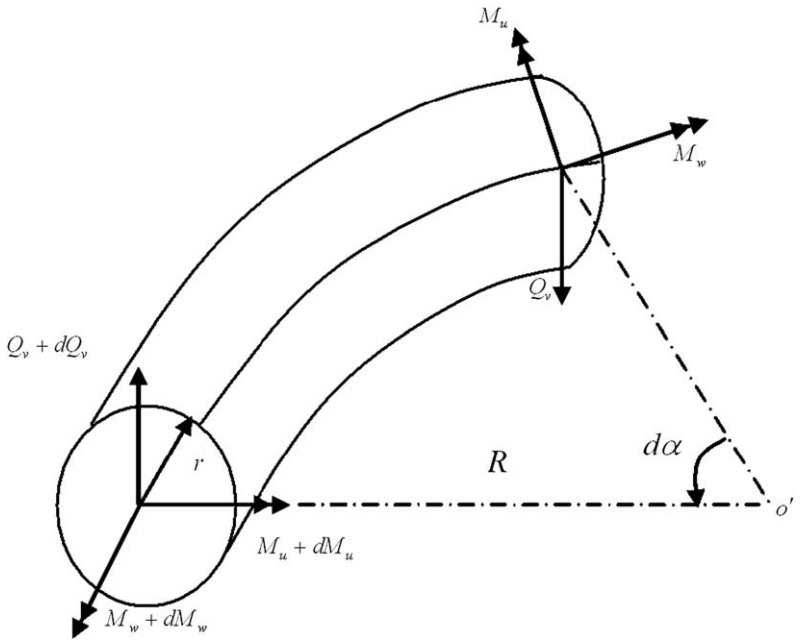


Fig. 5. Out-of-plane deformation and internal forces for an element of the ring.

Substituting Eq. (24) into (22), the equation governing the out-of-plane deformation $v$ can be obtained as follows:

$$\begin{aligned}
&\frac{\partial^6 v}{\partial\alpha^6}+2\frac{\partial^4 v}{\partial\alpha^4}+\frac{\partial^2 v}{\partial\alpha^2}-\rho AR^2\left(\frac{R^2}{C_w}+\frac{1}{k'AG}\right)\frac{\partial^2 v}{\partial t^2}-\rho^2R^4\left(\frac{I_u}{C_wk'G}+\frac{AI_wR^2}{EI_uC_w}+\frac{I_w}{EIk'G}\right)\frac{\partial^4 v}{\partial t^4}\\
&-\frac{\rho^3I_wR^6}{EC_wk'G}\frac{\partial^6 v}{\partial t^6}+\rho R^2\left(\frac{AR^2}{EI}-\frac{2}{k'G}+\frac{I_u}{C_w}+\frac{I_w}{EI_u}\right)\frac{\partial^4 v}{\partial t^2\partial\alpha^2}-\rho R^2\left(\frac{1}{E}+\frac{I_w}{C_w}+\frac{1}{k'G}\right)\frac{\partial^6 v}{\partial t^2\,\partial\alpha^4}\\
&+\rho^2R^4\left(\frac{1}{Ek'G}+\frac{I_w}{C_wk'G}+\frac{I_w}{EC_w}\right)\frac{\partial^6 v}{\partial t^4\,\partial\alpha^2}\\
&=-\frac{R}{k'AG}\frac{\partial^4 F_v}{\partial\alpha^4}+R\left(\frac{R^2}{EI_u}-\frac{2}{k'AG}\right)\frac{\partial^2 F_v}{\partial\alpha^2}-R\left(\frac{R^2}{C_w}+\frac{1}{k'AG}\right)F_v\\
&\frac{\rho R^3}{k'AG}\left(\frac{1}{E}+\frac{I_w}{C_w}\right)\frac{\partial^4 F_v}{\partial t^2\partial\alpha^2}-\rho R^3\left(\frac{I_u}{k'AGC_w}+\frac{I_wR^2}{EI_uC_w}+\frac{I_w}{k'AGEI_u}\right)\frac{\partial^2 F_v}{\partial t^2}-\frac{\rho^2I_wR^5}{k'AGEC_w}\frac{\partial^4 F_v}{\partial t^4}.
\end{aligned}\tag{25}$$

It is noted that the terms including the denominators containing the product of $E$ and $G$ in Eq. (25) are sufficiently small to be neglected. Thus Eq. (25) can be simplified into the following form

$$\begin{aligned}
&\frac{\partial^6 v}{\partial\alpha^6}+2\frac{\partial^4 v}{\partial\alpha^4}+\frac{\partial^2 v}{\partial\alpha^2}-\rho AR^2\left(\frac{R^2}{C_w}+\frac{1}{k'AG}\right)\frac{\partial^2 v}{\partial t^2}+\rho R^2\left(\frac{AR^2}{EI_u}-\frac{2}{k'G}+\frac{I_u}{C_w}+\frac{I_w}{EI_u}\right)\frac{\partial^4 v}{\partial t^2\partial\alpha^2}\\
&-\rho R^2\left(\frac{1}{E}+\frac{I_w}{C_w}+\frac{1}{k'G}\right)\frac{\partial^6 v}{\partial t^2\partial\alpha^4}=-\frac{R}{k'AG}\frac{\partial^4 F_v}{\partial\alpha^4}+R\left(\frac{R^2}{EI_u}-\frac{2}{k'AG}\right)\frac{\partial^2 F_v}{\partial\alpha^2}-R\left(\frac{R^2}{C_w}+\frac{1}{k'AG}\right)F_v
\end{aligned}\tag{26}$$

By the description in Section 2.2, the deformations of a closed ring can be expressed through the modal superposition method (Blevins, 1979). Thus the deformation can be expressed as

$$v=\sum_{i=2}^{J}[v_i^c(t)\cos(i\alpha)+v_i^s(t)\sin(i\alpha)],\tag{27}$$

where the subscript $i$ denotes the $i$th mode. Substituting Eq. (27) into Eq. (26) and utilizing the orthogonality of the trigonometric functions, the equations for each mode of deformation can be obtained as follows:

$$\begin{aligned}
&\rho\pi R^2\left[EI_u\left(\frac{AR^2}{GI_w}+\frac{1}{k'G}\right)+\left(AR^2-\frac{2EI_u}{k'G}+\frac{EI_uI_u}{GI_w}+I_w\right)i^2+\left(I_u+\frac{E}{G}+\frac{E}{k'G}\right)i^4\right]\frac{\partial^2 v_i^c}{\partial t^2}\\
&=R\left[\frac{EI_u}{k'AG}(i^2-1)^2+R^2\left(i^2+\frac{EI_u}{C_w}\right)\right]\int_0^{2\pi}F_v\cos(i\alpha)d\alpha-(i^3-i)^2EI_u\pi v_i^c,
\end{aligned}\tag{28}$$

and

$$\begin{aligned}
&\rho\pi R^2\left[\left(\frac{EI_uAR^2}{GI_w}+\frac{EI_u}{k'G}\right)+\left(AR^2-\frac{2EI_u}{k'G}+\frac{EI_uI_u}{GI_w}+I_w\right)i^2\right.\\
&\left.+\left(I_u+\frac{EI_u}{G}+\frac{EI_u}{k'G}\right)i^4\right]\frac{\partial^2 v_i^s}{\partial t^2}\\
&=R\left[\frac{EI_u(i^2-1)^2}{k'AG}+R^2\left(i^2+\frac{EI_u}{C_w}\right)\right]\int_0^{2\pi}F_v\sin(i\alpha)d\alpha-(i^3-i)^2EI_u\pi v_i^s.
\end{aligned}$$

Eq. (28) is used to compute the out-of-plane deformations $v$. Similarly the equations governing the two slopes $\phi_u$ and $\phi_w$ can be obtained according to the above deduction by combining Eq. (22) and Eq. (24). Here, the slopes are supposed to be $\phi_u=\sum_{i=2}^{J}[\varphi_i^s(t)\sin(i\alpha)+\varphi_i^c(t)\cos(i\alpha)]$ and $\phi_w=\sum_{i=2}^{J}[\xi_i^c(t)\cos(i\alpha)+\xi_i^s(t)\sin(i\alpha)]$, and the governing equations are given by

$$\begin{aligned}
&\rho R^2\left[I_u\left(\frac{EAR^2}{GI_w}+\frac{E}{k'G}\right)+\left(AR^2-\frac{2EI_u}{k'G}+\frac{EI_uI_u}{GI_w}+I_w\right)i^2+\left(I_u+\frac{EI_u}{G}+\frac{EI_u}{k'G}\right)i^4\right]\frac{\partial^2\varphi_i^s}{\partial t^2}\pi\\
&=iR^2\left(i^2+\frac{EI_u}{GI_w}\right)\int_0^{2\pi}F_v\cos(i\alpha)d\alpha-(i^3-i)^2EI_u\pi\varphi_i^s,
\end{aligned}\tag{29}$$

and

$$\rho R^2\left[\left(\frac{EI_uAR^2}{GI_w}+\frac{EI_u}{k'G}\right)+\left(AR^2-\frac{2EI_u}{k'G}+\frac{EI_uI_u}{GI_w}+I_w\right)i^2+\left(I_u+\frac{EI_u}{G}+\frac{EI_u}{k'G}\right)i^4\right]\frac{\partial^2\varphi_i^c}{\partial t^2}\pi$$
$$=-iR^2\left(i^2+\frac{EI_u}{GI_w}\right)\int_0^{2\pi}F_v\sin(i\alpha)d\alpha-(i^3-i)^2EI_u\pi\varphi_i^c;$$

$$\rho\pi R^2\left[\left(\frac{EI_u}{k'G}+\frac{EI_uAR^2}{GI_w}\right)+\left(AR^2-\frac{2EI_u}{k'G}+I_w+\frac{EI_uI_u}{GI_w}\right)i^2+\left(\frac{EI_u}{k'G}+I_u+\frac{EI_u}{G}\right)i^4\right]\frac{\partial^2\xi_i^c}{\partial t^2}$$
$$=-i^2R^2\left(1+\frac{EI_u}{GI_w}\right)\int_0^{2\pi}F_v\cos(i\alpha)d\alpha-(i^3-i)^2EI_u\pi\xi_i^c \tag{30}$$

and

$$\rho R^2\left[\left(\frac{EI_u}{k'G}+\frac{EI_uAR^2}{GI_w}\right)+\left(AR^2-\frac{2EI_u}{k'G}+I_w+\frac{EII_u}{GI_{w\,u}}\right)i^2+\left(\frac{EI_u}{k'G}+I_u+\frac{EI_u}{G}\right)i^4\right]\frac{\partial^2\xi_i^s}{\partial t^2}\pi$$
$$=-i^2R^2\left(1+\frac{EI_u}{C_w}\right)\int_0^{2\pi}F_v\sin(i\alpha)d\alpha-(i^3-i)^2EI_u\pi\xi_i^s.$$

Eqs. (28), (29) and (30) are used to solve the out-of-plane deformations of the ring.

Combining the equations of the rigid-body motions of the ring (3), (6), (7), (8), (9) and (10) and deformation equations, including in-plane ones (19) and (21) and out-of-plane ones (28), (29) and (30), the displacements of the ring, the internal forces and stress on the cross-section of the ring can be solved numerically.

## 3. Wave forces predicted by the Morison formula

The diameter of the cross-section of a flotation ring is much smaller than the wavelength, making the wave diffraction effect negligible. The wave forces acting on the ring, therefore, can be evaluated from the Morison formula. The Morison formula is a well-known equation, initially proposed for calculating the flow forces on a slender vertical member in surface waves. However, the centerline of the element of the ring is inclined to the advancing direction of waves, and the ring oscillates with the water waves. Here, the form of the Morison formula given by Brebbia and Walker (1979) is employed, as in Eq. (31). In the formula, the drag force is related to the square of the relative velocity of a water particle to an element of the ring, and the added mass force and inertia force are proportional to the acceleration of the water particle and that relative to an element of the ring, respectively:

$$\vec{f}=\rho_wC_DS\frac{\vec{V}_{\rm rel}|\vec{V}_{\rm rel}|}{2}+\rho_wK_mV_f\frac{\partial\vec{V}_{\rm rel}}{\partial t}+\rho_wV_f\frac{\partial\vec{V}}{\partial t}, \tag{31}$$

where $\vec{V}$ denotes the velocity of the water particle obtained from the second-order wave theory (see Appendix 2), $\vec{V}_{\rm rel}$ denotes the velocity of the water particle relative to the member, $C_D$ and $K_m$ are the empirical coefficients, $\rho_w$ the mass density of water and $S$ the projected areas of the element of the ring per unit length immersed in water. Due to the changing angle between the centerline of the element of the ring and the advancing direction of waves, we calculate the wave forces in the $n$–$w$–$v$ coordinate system. The projected areas of the ring per unit length $S_u$, $S_w$ and $S_v$ along the $n$-, $w$- and $v$-axis are given by

$$S_u=\begin{cases}2r\\ r+h\\ r-h\\ 0\end{cases},\quad S_w=\begin{cases}2r\\ r+2r\arcsin(|h|/r)/\pi\\ r-2r\arcsin(|h|/r)/\pi\\ 0\end{cases},\quad S_v=\begin{cases}2r & h\ge r\\ 2r & 0\le h\le r\\ 2\sqrt{r^2-h^2} & -r\le h\le 0\\ 0 & h\le -r\end{cases}\text{ when}. \tag{32}$$

## 4. Results and discussion

Reasonable values of hydrodynamic coefficients are pre-fixed by comparison between the numerical results of the rigid-body displacements of the ring and experimental data. The physical model tests were conducted by Gui (2006),

with the waves propagating along the $x$-axis. The multi-directional waves acting on the ring are then analyzed to show the influence of hydroelasticity. In the numerical examples, gravity acceleration $g$ is set as $9.8\,m/s^2$, and the density of water is $1000\,kg/m^3$. The fourth-order Runge–Kutta algorithm is used to solve the differential equations governing the deformations and motions, and the numerical calculation is processed by programming with Fortran Language. In the calculation, the ring is subdivided into 400 arc subsections to calculate the integral in the equations, and the time step is equal to three-thousandths of the wave period. The calculation will stop when the history of one period is very close to that of the subsequent period.

### 4.1. Description of physical model tests

The physical model tests of a gravity-type fish cage were conducted in a wave-current flume at the State Key Laboratory of Coastal and Offshore Engineering, Dalian University of Technology, China. The wave-current flume is 69 m long, 2 m wide and 1.8 m high, equipped with an irregular wave-maker and a current-producing system. The incident waves propagated along the positive $x$-direction. The mooring line forces were measured by two transducers attached to the bottom of each mooring lines. Three diodes (front, middle and back) numbered 1, 2 and 3 were fixed on the floating system for motion analysis. The movement of diodes was recorded by a CCD camera, maximum relative error of the measurements of which was less than 10% (Gui et al., 2006).

The configuration of the net cage in model tests is shown in Fig. 1. The radius of the ring and cross-sectional radius are 0.423 and 0.00766 m, respectively. The modulus of elasticity of the material of the flotation ring is $9.0\times10^8$ Pa, and its density is $953\,kg/m^3$. The mooring cable is simulated using nylon line. Fitting of this experimental data yields the following empirical formula relating the elongation and the force of the mooring line

$$F_{1A}=\begin{cases}-360.21\varepsilon^2+82.9\varepsilon & \text{when} \quad l>l_0\\ 0 & \text{when} \quad l\le l_0\end{cases} \quad \text{where} \quad \varepsilon=\frac{l-l_0}{l_0}; \tag{33}$$

$l_0$ is the initial length of the mooring cable, and $l$ its length when the model fish cage is moving. In the physical model tests, twelve cases covering four wave heights (0.2, 0.25, 0.29 and 0.034 m) and five periods ( 1.2, 1.4, 1.6, 1.8 and 2.0 s) were considered.

In our numerical calculation, the maximum of the mode $J$ is equal to 5. A numerical example is given as follows: when the wave height and period are 0.34 m and 2.0 s, respectively, the maximum values ($\tau_J$) of tangent deformations under each mode $J$ ($J=2$–5) are $3.85\times10^{-4}$, $1.35\times10^{-5}$, $3.18\times10^{-6}$ and $1.21\times10^{-6}$ m, respectively. It can be found that the response contributed by the second mode is much larger than that by the fifth mode. When the mode number $J$ is greater than 5, the response contributed by the mode becomes negligible. The same results can also be found in the out-of-plane on deformation and slopes. Here, the maximum of the mode $J$ is set at 5.

### 4.2. Comparison of theoretical results and experimental data

To compute the wave forces from the Morison formula, the values of hydrodynamic coefficients $C_D$ and $K_m$ should be pre-fixed. Li et al. (2007) investigated the hydrodynamic behavior of a straight floating pipe, and suggest a range of the hydrodynamic coefficients. Referring to the research of Li et al. (2007), $C_{Dn}$ and $C_{Dv}$ are set as 0.5 each, and $C_{Dw}$ and $K_m$ are set as 0.16 and 0.2, respectively. With these values substituting into the Morison formula, the theoretical model presented in Section 3 is applied to simulate the physical model tests (Gui, 2006). Waves propagate along the positive direction of the $x$-axis, which means that the propagation angle $\sigma$ of incident wave is equal to zero. Additionally, the velocity potential is given according to second-order wave theory. The wave surface elevation, the velocities and accelerations of water particle can then be obtained by wave theory in Appendix 2. In Fig. 6, hollow points represent the average of the maximum positive displacements of surge and heave on the consecutive water waves through the experimental measurement, and solid points depict the numerical results. It can be seen that the predicted results of surge and heave displacements are all in agreement with the experimental data. The maximum of the relative error between simulated and measured data is 15%. As shown in the Fig. 6, the error between simulated and measured data is larger when the wave height becomes larger. This phenomenon may be due to neglecting the nonlinear effects of both waves and the mooring line in our present numerical model, which will be improved in our future research.

### 4.3. Elastic response

In the experimental model tests mentioned above, the similarity of the modulus of elasticity is not fully considered because it is difficult to find the appropriate material with a modulus of elasticity fully in accord with the demand of the

physical model tests. In this section, the floating ring in a prototype dimension is considered and simulated. The radius of the ring is 8.46 m, the radius and the wall depth of the cross-section of the ring are 0.125 and 0.013 m, respectively, and the modulus of elasticity is still $9.0 \times 10^8$ Pa. The initial length of mooring cable is 63.27 m, while the coordinate of attachment points A, B, C and D in the global coordinate system is (64.5, 19.4, −20.0 m), (−64.5, 19.4, −20),

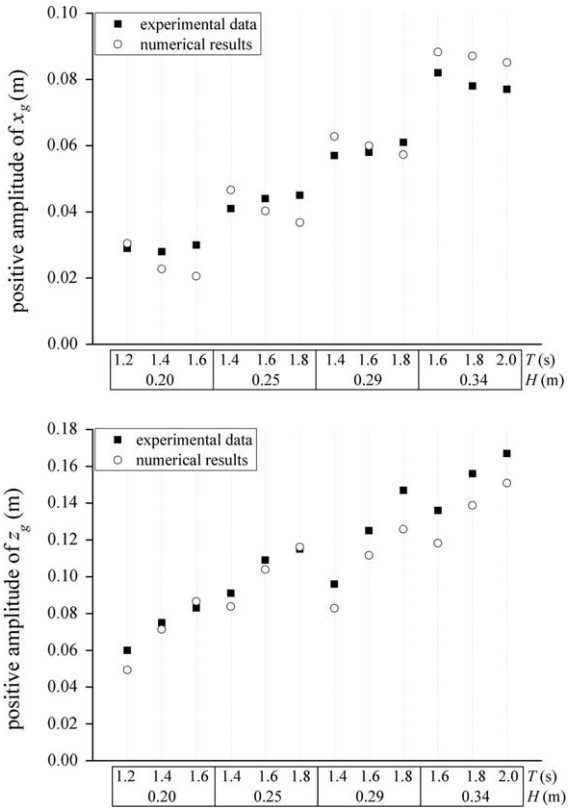


Fig. 6. Comparison of the predicted results with the experimental data for $x_g$ (top) and $z_g$ (below).

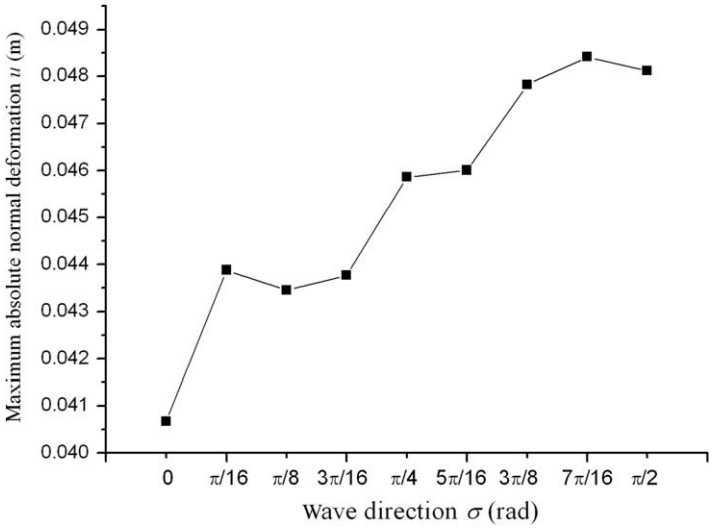


Fig. 7. Responses of the maximum absolute normal deformations with different wave directions.

(−64.5, −19.4, −20.0 m) and (64.5, −19.4, −20.0 m). The relationship between the force and the elongation of the mooring line is set as follows:

$$F_{1A} = \begin{cases} 372494.08\varepsilon^{1.037} & \text{when} \quad l > l_0 \\ 0 & \text{when} \quad l \le l_0 \end{cases} \quad \text{where} \quad \varepsilon = \frac{l - l_0}{l_0}, \tag{34}$$

which is an empirical formula, and it can also be given according to the real measurements.

Firstly, the influence of the propagation angle $\sigma$of the incident wave is analyzed, while the wave height is 2.0 m, and wave period is 20.0 s. The angle $\sigma$ increases from 0 to $\pi/2$ at an interval of $\pi/16$. Figs. 7–9 represent the maximum absolute values of normal, circumferential, and out-of-plane deformations. It can be seen that the minimum magnitude of deformations, including in-plane and out-of-plane ones, will occur when $\sigma$ is 0. It also means that the ring deforms most weakly when the incident wave propagates along the $x$-axis. Therefore, the placement of a fish cage is recommended to be configured in the direction of the principal axis of which is parallel to the wave direction.

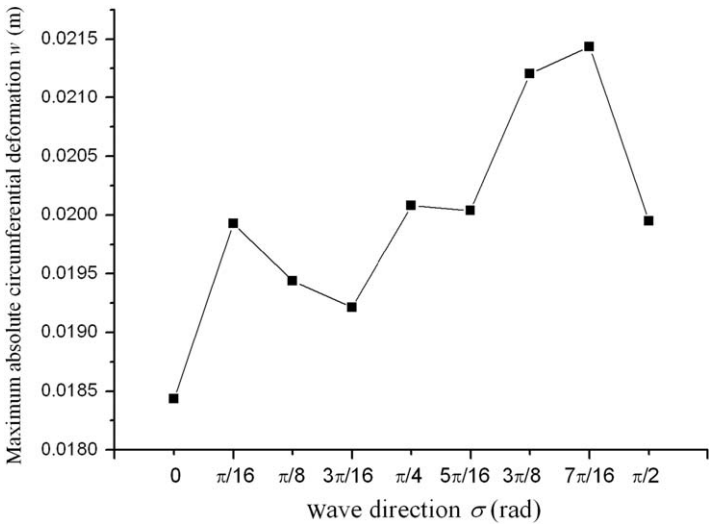


Fig. 8. Responses of the maximum absolute circumferential deformations with different wave directions.

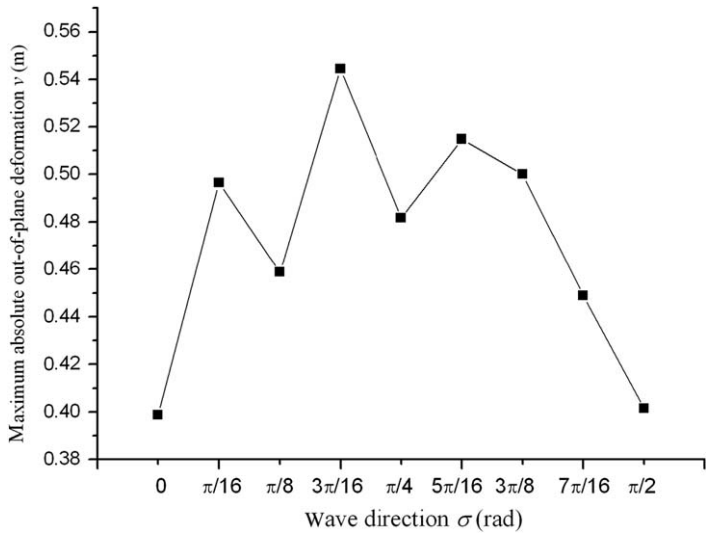


Fig. 9. Responses of the maximum absolute out-of-plane deformations with different wave directions.

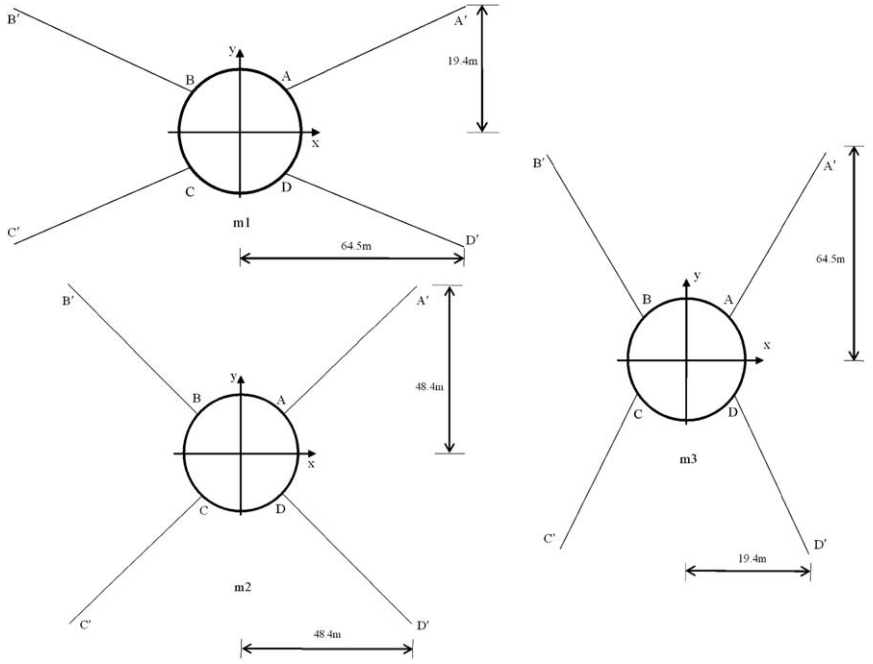


Fig. 10. Sketch of three kinds of mooring arrangments (m1, m2, and m3).

Table 1
The maximum absolute deformations with different configurations of mooring cables.

| Configuration of mooring cables | Maximum absolute normal deformation (m) | Maximum absolute circumferential deformation (m) | Maximum absolute out-of-plane deformation (m) |
|---|---|---|---|
| m1 | 0.040668 | 0.018434 | 0.398737 |
| m2 | 0.009399 | 0.002694 | 0.406882 |
| m2 | 0.048172 | 0.019968 | 0.401414 |

Additionally, comparing the out-of-plane deformations and the in-plane ones (see Figs. 7–9), it can be seen that the magnitude of $v$ is much larger than that of $n$ and $w$. It can be concluded that the out-of-plane breakage of the ring would occur prior to the in-plane one.

Secondly, the effect of the different kinds of arrangements of mooring lines is analyzed. Besides the above form shown in Fig. 1, in which the attachment points A, B, C and D in the global coordinate system are another form of the ordinates of anchored points is considered: (19.4, 64.5, −20.0 m), (−19.4, 64.5, −20.0 m), (−19.4, −64.5, −20.0 m) and (19.4, −64.5, −20.0 m). The above two forms are named "m1" and "m3". The form "m2" is that the attachment points A, B, C and D in the global coordinate system being set as (48.4, 48.4, −20 m), (−48.4, 48.4, −20 m), (−48.4, −48.4, −20 m) and (48.4, −48.4, −20 m). The configurations of the three types of mooring arrangement are shown in Fig. 10. It is notable that the initial lengths of mooring line are the same.

The maximum absolute deformations are listed in Table 1. It can be found that under the mooring arrangement "m2", in-plane deformations of the ring are smaller than the other two kinds of arrangements. For out-of-plane deformations, the distinctions among the three kinds of arrangements are small.

According to the above theoretical analysis, a viable scheme of the fish cage arrangement can be obtained. It is suggested that it is better if the cage is moored by symmetric mooring cables around two principal axes, and that a principal axis is parallel to wave incident direction. It is also noted that the out-of-plane deformations are much larger than the in-plane one.

In order to examine the validity of the calculated elastic response, the static deformation of a circular ring calculated by our analytical method has been validated by comparison with the calculated results by ANSYS software. The details

of the validation have been published previously (Zong et al., 2008). In our future research, more calculations and physical tests have been planned to obtain the elastic response of the ring for validation of the method.

## 5. Conclusions

A theoretical analysis for evaluating the rigid-body motions of the ring subjected to water waves is presented, coupled with elastic deformations. The predicted results of rigid-body displacements are compared with the experimental data, with acceptable correlation between numerical results and experimental data. The elastic responses of a ring under different incident wave directions and mooring arrangements are calculated and analyzed. Based on the simulated results, some useful suggestions on mooring arrangements and placement of the fish cage are obtained.

## Acknowledgements

This research was financially supported by the National High-Tech Research and Development Program of China (Grant nos. 2006AA100301), the National Natural Science Foundation of China (Grant no. 50809014, 50921001 and 50579004), and Specialized Research Fund for the Doctoral Program of Higher Education (Grant no. 200801411094).

## Appendix 1

Bryant angles are the common parameters used to describe the angular orientation of a body in space. The angular orientation of a given body-fixed coordinate system 1–2–3 can be envisioned to be the result of three successive rotations. The three angles of rotation corresponding to the three successive rotations are defined as Bryant angles.

The first rotation may be carried out counterclockwise about the $x$-axis through an angle $\theta_1$; the resultant coordinate system will be labeled $x'-y'-z'$, as shown in Fig. 11. The second rotation, through an angle $\theta_2$ counterclockwise about the $y'$ axis, produces the coordinate system. Finally, the third rotation, counterclockwise about the $z''$ axis through an angle $\theta_3$, results in the 1–2–3 coordinate system. The transformation matrices for the individual rotations are

$$\begin{bmatrix} 1 & 0 & 0 \\ 0 & \cos\theta_1 & \sin\theta_1 \\ 0 & -\sin\theta_1 & \cos\theta_1 \end{bmatrix}, \begin{bmatrix} \cos\theta_2 & 0 & -\sin\theta_2 \\ 0 & 1 & 0 \\ \sin\theta_2 & 0 & \cos\theta_2 \end{bmatrix}, \begin{bmatrix} \cos\theta_3 & \sin\theta_3 & 0 \\ -\sin\theta_3 & \cos\theta_3 & 0 \\ 0 & 0 & 1 \end{bmatrix}. \tag{35}$$

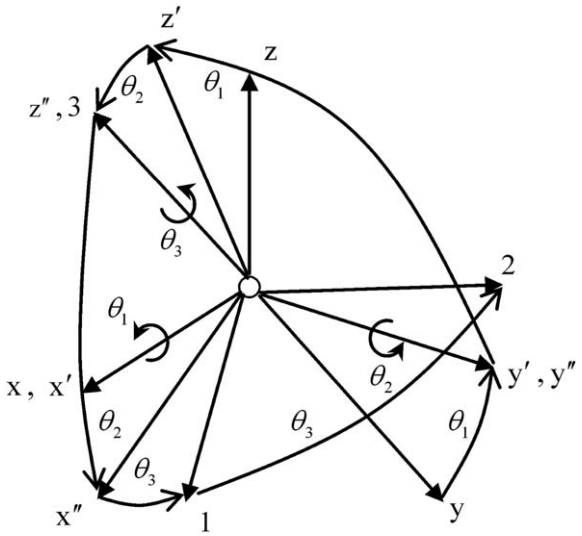


Fig. 11. Schematic diagram of Bryant angles.

Hence, the matrix of the complete transformation, Eq. (2), is

$$\begin{bmatrix} \cos\theta_2\cos\theta_3 & \cos\theta_1\sin\theta_3+\sin\theta_1\sin\theta_2\cos\theta_3 & \sin\theta_1\sin\theta_3-\cos\theta_1\sin\theta_2\cos\theta_3 \\ -\cos\theta_2\sin\theta_3 & \cos\theta_1\cos\theta_3-\sin\theta_1\sin\theta_2\sin\theta_3 & \sin\theta_1\cos\theta_3+\cos\theta_1\sin\theta_2\sin\theta_3 \\ \sin\theta_2 & -\sin\theta_1\cos\theta_2 & \cos\theta_1\cos\theta_2 \end{bmatrix}. \tag{36}$$

## Appendix 2

A second-order wave theory (Stoker, 1957) is employed to calculate the velocity and acceleration of a water particle. Suppose that wave height is $H$. The fluctuating wave surface height $\eta$ is given by

$$\eta=\frac{H}{2}\left[-\frac{H}{2}\frac{k}{2\sinh 2kd}+\cos(k_x x+k_y y-\omega t)+\frac{H}{2}\frac{k}{4}\frac{\cosh kd(2\cosh^2 kd+1)}{\sinh^3 kd}\cos 2(k_x x+k_y y-\omega t)\right], \tag{37}$$

where $\omega$ is the circular frequency, $k$ the wave number, $d$ the wave depth and $k_x$ the component of wave number along the $x$-axis, $k_x=k\cos\sigma$, and $k_y$ the component of wave number along $y$-axis, $k_y=k\sin\sigma$.

The horizontal and vertical velocities of a water particle are

$$V_x=\omega\frac{k_x}{k}\frac{H}{2}\left[\frac{\cosh k(z+d)}{\sinh kd}\cos(k_x x+k_y y-\omega t)+\frac{3}{4}k\left(\frac{H}{2}\right)\frac{\cosh 2k(z+d)}{(\sinh kd)^4}\cos 2(k_x x+k_y y-\omega t)\right], \tag{38}$$

$$V_y=\omega\frac{k_y}{k}\frac{H}{2}\left[\frac{\cosh k(z+d)}{\sinh kd}\cos(k_x x+k_y y-\omega t)+\frac{3}{4}k\left(\frac{H}{2}\right)\frac{\cosh 2k(z+d)}{(\sinh kd)^4}\cos 2(k_x x+k_y y-\omega t)\right], \tag{39}$$

$$V_z=\omega\frac{H}{2}\left[\frac{\sinh k(z+d)}{\sinh kd}\sin(k_x x+k_y y-\omega t)+\frac{3}{4}\frac{H}{2}k\frac{\sinh 2k(z+d)}{\sinh^4 kd}\sin 2(k_x x+k_y y-\omega t)\right]. \tag{40}$$

The horizontal and vertical accelerations of a water particle, therefore, can be given by

$$\frac{\partial V_x}{\partial t}=\omega^2\frac{k_x}{k}\frac{H}{2}\left[\frac{\cosh k(z+d)}{\sinh kd}\sin(k_x x+k_y y-\omega t)+\frac{3}{2}k\left(\frac{H}{2}\right)\frac{\cosh 2k(z+d)}{(\sinh kd)^4}\sin 2(k_x x+k_y y-\omega t)\right], \tag{41}$$

$$\frac{\partial V_y}{\partial t}=\omega^2\frac{k_y}{k}\frac{H}{2}\left[\frac{\cosh k(z+d)}{\sinh kd}\sin(k_x x+k_y y-\omega t)+\frac{3}{2}k\left(\frac{H}{2}\right)\frac{\cosh 2k(z+d)}{(\sinh kd)^4}\sin 2(k_x x+k_y y-\omega t)\right], \tag{42}$$

$$\frac{\partial V_z}{\partial t}=-\omega^2\frac{H}{2}\left[\frac{\sinh k(z+d)}{\sinh kd}\cos(k_x x+k_y y-\omega t)+\frac{3}{2}\frac{H}{2}k\frac{\sinh 2k(z+d)}{\sinh^4 kd}\cos 2(k_x x+k_y y-\omega t)\right]. \tag{43}$$

## References


Blevins, R.D., 1979. Formulas for Natural Frequency and Mode Shape. Van Nostrand Reinhold Company, New York, pp. 203–206.

Brebbia, C.A., Walker, S., 1979. Dynamic Analysis of Offshore Structures. Newnes-Butterworths, London.

Chaplin, J.R., Retzler, C.H., 2001. Hydrodynamic damping of the vertical motion of a horizontal cylinder beneath waves at large scale. Journal of Fluids and Structures 15, 929–940.

DeCew, J., Fredriksson, D.W., Bugrov, L., et al., 2005. A case study of a modified gravity type cage and mooring system using numerical and physical models. IEEE Journal of Oceanic Engineering 30 (1), 47–58.

Fredriksson, D.W., 2001. Open ocean fish cage and mooring system dynamics. Ph.D. dissertation, University of New Hampshire, Durham, USA.

Fredriksson, D.W., DeCewb, J.C., Tsukrov, I., 2007. Development of structural modeling techniques for evaluating HDPE plastic net pens used in marine aquaculture. Ocean Engineering 34, 2124–2137.

Galper, A.R., Miloh, T., 2000. Hydroelasticity of the kirchhoff rod: buckling phenomena. Journal of Fluids and Structures 14, 1089–1100.

Gui, F.K., 2006. Hydrodynamic behaviors of deep-water gravity cage. Ph.D. Dissertation, Dalian University of Technology, Dalian (in Chinese).

Gui, F.K., Li, Y.C., Dong, G.H., et al., 2006. Application of CCD image scanning to sea-cage motion response analysis. Aquacultural Engineering 35, 179–190.

Huang, C.C., Tang, H.J., Liu, J.Y., 2006. Dynamical analysis of net cage structures for marine aquaculture: numerical simulation and model testing. Aquacultural Engineering 35, 258–270.

Li, Y.C., Gui, F.K., Teng, B., 2007. Hydrodynamic behavior of a straight floating pipe under wave conditions. Ocean Engineering 34, 552–559.

Li, Y.S., Zhan, S., Lau, S.L., 1997. In-line response of a horizontal cylinder in regular and random waves. Journal of Fluids and Structures 11, 73–87.

Stoker, J.J., 1957. Water Waves: The Mathematical Theory with Applications. Interscience Publishers, New York.

Wittenburg, J., 1977. Dynamics of systems of rigid bodies. B.G. Teubner, Stuttgart.

Zong, Z., Hao, S.H., Zhao, Y.P., 2008. In-plane hydroelastic response of a circular ring in water waves. Applied Ocean Research 30 (3), 208–214.